Bmp2 in osteoblasts of periosteum and trabecular bone links bone formation to vascularization and mesenchymal stem cells

Wuchen Yang[1,2], Dayong Guo[3,4], Marie A. Harris[1], Yong Cui[1], Jelica Gluhak-Heinrich[1], Junjie Wu[5], Xiao-Dong Chen[5], Charles Skinner[5], Jeffry S. Nyman[6], James R. Edwards[6], Gregory R. Mundy[6,*], Alex Lichtler[7], Barbara E. Kream[7], David W. Rowe[7], Ivo Kalajzic[7], Val David[8], Darryl L. Quarles[8], Demetri Villareal[1], Greg Scott[9], Manas Ray[9], S. Liu[10], James F. Martin[11], Yuji Mishina[12] and Stephen E. Harris[1,‡]

[1]Department of Periodontics, University of Texas Health Science Center at San Antonio, San Antonio, TX 78229, USA
[2]Department of Craniofacial Sciences, University of Connecticut Health Center, Farmington, CT 06030, USA
[3]Department of Oral Biology, University of Missouri at Kansas City, Kansas City, MO 64108, USA
[4]Regeneron Inc., Tarrytown, NY 10591, USA
[5]Department of Comprehensive Dentistry, University of Texas Health Science Center at San Antonio, San Antonio, TX 78229, USA
[6]Department of Orthopaedic Surgery and Rehabilitation and Vanderbilt Center for Bone Biology, Vanderbilt University Medical Center, Nashville, TN 37232, USA
[7]Center for Regenerative Medicine and Skeletal Development, University of Connecticut Health Center, Farmington, CN 06030, USA
[8]Department of Medicine, University of Tennessee Health Science Center, Memphis, TN 38104, USA
[9]National Institute of Environmental Health Sciences, Research Triangle Park, NC 27709, USA
[10]Endocrine and Renal Science, Genzyme Co., Framingham, MA 01701, USA
[11]Department of Molecular Physiology and Biophysics, Baylor College of Medicine, Houston, TX 77030, USA
[12]Department of Biologic and Material Sciences, School of Dentistry, University of Michigan, Ann Arbor, MI 48109, USA

*Deceased
‡Author for correspondence (harris@uthscsa.edu)

Accepted 10 June 2013
Journal of Cell Science 126, 4085–4098

doi: 10.1242/jcs.118596

Summary

We generated a new *Bmp2* conditional-knockout allele without a neo cassette that removes the *Bmp2* gene from osteoblasts (Bmp2-cKO^{ob}) using the 3.6Col1a1-Cre transgenic model. Bones of Bmp2-cKO^{ob} mice are thinner, with increased brittleness. Osteoblast activity is reduced as reflected in a reduced bone formation rate and failure to differentiate to a mature mineralizing stage. Bmp2 in osteoblasts also indirectly controls angiogenesis in the periosteum and bone marrow. VegfA production is reduced in Bmp2-cKO^{ob} osteoblasts. Deletion of *Bmp2* in osteoblasts also leads to defective mesenchymal stem cells (MSCs), which correlates with the reduced microvascular bed in the periosteum and trabecular bones. Expression of several MSC marker genes (α-SMA, CD146 and Angiopoietin-1) *in vivo*, *in vitro* CFU assays and deletion of *Bmp2 in vitro* in α-SMA^{+} MSCs support our conclusions. Critical roles of *Bmp2* in osteoblasts and MSCs are a vital link between bone formation, vascularization and mesenchymal stem cells.

Key words: Bmp2, Osteoblasts, Angiogenesis, Mesenchymal stem cells, VegfA, α-SMA+ cells

Introduction

The bone morphogenic protein (BMP) signaling pathway is important for developmental and postnatal physiological processes (Bonilla-Claudio et al., 2012; Dutko and Mullins, 2011; Sieber et al., 2009; Watabe and Miyazono, 2009; Yoon et al., 2005; Zhao et al., 2002). BMP signaling pathways are common for BMP ligands and involve three different type I BMP receptors and two different type II receptors plus negative regulators of BMP signaling, such as noggin and gremlin (Dutko and Mullins, 2011). Selected polymorphisms in the *BMP2* gene are associated with increased fracture risk and osteoporosis (Styrkarsdottir et al., 2003). Deletion of other BMP family members *Bmp7* and *Bmp4* suggests that they play minor roles in bone and cartilage development in the embryo or postnatally, whereas *Bmp2* is critical for chondrocyte function and endochondral bone development (Bandyopadhyay et al., 2006; Shu et al., 2011; Tsuji et al., 2008). Removal of *Bmp2* in mouse mesenchymal precursor cells in 10 d.p.c. embryos shows a minor role for Bmp2 during endochondral bone formation, but adult mice have small bones that show an increased fracture risk and failure to heal (Tsuji et al., 2006).

Vascularization and angiogenesis are linked to cartilage and bone formation and to fracture healing (Araldi and Schipani, 2010; Jacobsen et al., 2008; Maes et al., 2012; Schipani et al., 2009). During aging or glucocorticoid treatment, bone angiogenesis is reduced and brittleness in bone is increased (Weinstein, 2010; Weinstein et al., 2010). VegfA overexpression in bone marrow leads to formation of new bone and associated blood vessels (Maes et al., 2010a). BMP signaling in osteoblasts increases VegfA through Osterix and Runx2/Hif1a (Deckers et al., 2002; Kwon et al., 2011; Maes et al., 2012; Zhang et al., 2009). Recently, Liu and colleagues (Liu et al., 2012) demonstrated that VegfA is required in the progression of osteoblast precursors (Osterix^{+}) to mature osteoblasts.

Mesenchymal stem cells (MSCs) from both the periosteum and bone marrow, are progenitors of osteoblasts (Bianco et al., 2010; Schipani and Kronenberg, 2008) and express CD146 and α-SMA. MSCs are associated with microvascular structures in bone (Crisan et al., 2008; Grcevic et al., 2012; Sacchetti et al., 2007). α-SMA$^+$ cells isolated by lineage tracing studies are a class of MSCs that differentiate into osteoblasts (Grcevic et al., 2012). Osterix$^+$ preosteoblasts, which represent a non-proliferating transient state, move into bone marrow in association with vascular structures during bone development (Maes et al., 2010b; Park et al., 2012).

Bmp2 expression is activated in MSCs (smooth muscle cells α-SMA$^+$) on new induced blood vessels during bone formation and angiogenesis that is activated during distraction osteogenesis (Matsubara et al., 2012). There is first, rapid new blood vessel and associated candidate MSC formation, followed by new bone formation at the distraction site. From the above observations, we hypothesize that the *Bmp2* gene has multiple roles at different stages of osteogenesis, ranging from a requirement for terminal differentiation to driving vascularization and formation of new MSCs.

In these studies we: (1) characterized the bone phenotype in a Bmp2-cKO^{ob} model in both the periosteum and in the bone marrow, including histomorphometry; (2) mechanically tested the long bones to evaluate bone quality; (3) performed *in situ* hybridization and immunocytochemistry of the key genes and proteins involved in osteoblast and vascular biology; (4) created 3D vascular maps of the vascular bed in both the periosteum and bone marrow; (5) performed *in vitro* tests for cell autonomy of MSC number and their capacity to differentiate into osteoblasts; and (6) performed *in vitro* testing of Bmp2 function by deletion of *Bmp2* in enriched MSCs.

Results

Skeletal phenotype after *Bmp2* gene ablation from early osteoblasts in Bmp2-cKO^{ob} mice

Fig. 1A and supplementary material Fig. S1C show that *Bmp2* expression was reduced by 85–90% in the osteoblasts at 5 days, 1 month and 4 months in periosteum and trabecular bones (Yang et al., 2012). Bmp2 protein levels were also greatly reduced in osteoblasts (Fig. 1B). The body weight of the Bmp2-cKO^{ob} mouse changed little as assayed to 6 months (supplementary material Fig. S1D, top panel). Humerus length showed a 5% decrease at 2 weeks with no change between control and Bmp2-cKO^{ob} at 2–4 months (supplementary material Fig. S1D, bottom panel). Alizarin Red and Alcian Blue staining of newborns showed the skeleton was normal in the Bmp2-cKO^{ob} animals, with a slight decrease in the overall size of the vertebrae compared with heterozygotes or WT controls (supplementary material Fig. S2). The 3.6Col1a1-Cre is active in embryonic tissues that express type 1 collagen (E15–E19) as we and others have observed with Rosa26–*loxP*–Stop–*loxP*–*lacZ* assays, and this suggests that the *Bmp2* gene is minimally required in embryonic Col1a1-expressing tissues for proper development. Another possibility is that maternal Bmp2 crosses the placenta to rescue potential embryo stage bone phenotypes, which would minimize the bone phenotype. Maternal Bmp2 can play a role in embryonic phenotypes, as we have shown (Singh et al., 2008).

Two weeks after birth, Bmp2-cKO^{ob} mice had thinner bones and smaller unfused vertebrae with a 5% decrease in length compared with controls (WT or Hets) [supplementary material Fig. S1E (bottom right) and Fig. S2 (bottom panels)]. With time, the bone osteopenic-like phenotype, with thinner bones in the Bmp2-cKO^{ob} became progressively advanced, as assayed by digital radiography up to 1 year of age (Fig. 1C). We focused on males for statistical evaluation, and phenotypes were similar in females and males by X-ray analysis.

As analyzed by dynamic bone formation rate, both mineralizing surface (MS/BS=active surface area) and the mineral apposition rate (MAR, rate of new mineral deposition) were reduced by 20% in both the bone marrow trabeculae (Fig. 1D, top) and in the periosteum (Fig. 1D, bottom), leading to a 40% overall decrease in bone formation rate (BFR). BFR in the periosteum of femurs also showed a 40% decrease in 2-month-old Bmp2-cKO^{ob} compared with controls (data not shown).

μCT analysis of vertebrae and long bones at 4 months (n=5 per group) shows vertebrae are smaller by 35% in the Bmp2-cKO^{ob} with an unfused dorsal region (Fig. 2A). We observed an increase in rod-like quality of trabeculae of the Bmp2-cKO^{ob}. A 40% reduction in bone volume to total volume (BV/TV) was found in the trabecular region, as well as a 20% decrease in trabecular thickness. The tibia, femur and humerus showed a 30–40% decrease in bone volume compared with controls, but similar cortical thickness (data not shown).

Apparent bone mineral density (aBMD) from 2 weeks to 8 months of age demonstrated a progressive decrease in aBMD with age, especially in the spine (20% decrease in L4–L6 region) at 25 weeks and a 14–16% decrease in tibia and femur of Bmp2-cKO^{ob} (Fig. 2B). At 6 and 8 months, a similar 20% decrease in the spine aBMD was noted.

Mechanical and material properties indicate that Bmp2-cKO^{ob} bones are more brittle

By three-point bending of femurs and resulting stress–strain or force–displacement curves, we demonstrated a 40% decrease in stiffness and 50% decrease in work to fracture (W_f) (Fig. 2C) in the Bmp2-cKO^{ob} bones. Overall toughness of the bones was also decreased 35% in Bmp2-cKO^{ob} bones (Fig. 2C, top right). Post-yield toughness in Bmp2-cKO^{ob} bones was decreased by 75% (Fig. 2C, bottom right), demonstrating that the bones are much more brittle.

Histomorphometric and gene expression analysis demonstrates a failure in osteoblast differentiation

There were many flat and immature osteoblasts and fewer mature cuboidal polarized osteoblasts in Bmp2-cKO^{ob} compared with control littermates, as assayed from 5 days to 6 months (Fig. 3A and supplementary material Fig. S3A). By 8 weeks, there is an 80% decrease in the region of mature osteoblasts covering the bone surface and a decreased number of mature osteoblasts per bone surface, OB.S/BS and N.OB/BS (Fig. 3A, bottom left and supplementary material Fig. S3A), respectively. We observed no significant change in the osteoclasts (TRAP+ multinucleated cells, red stain) covering bone surfaces (OC.S/BS) or the number of osteoclasts per unit of bone surface (N.OC/BS) after 2 weeks of age. At 2 weeks, we noted a 10–15% decrease in OC.S/BS and N.OC/BS in the Bmp2-cKO^{ob} (Fig. 3A, bottom right and supplementary material Fig. S3A, right), respectively.

Osterix, Collagen Type 1a1 (Col1a1) and Osteocalcin expression is reduced by 80% in femurs of 5-day-old Bmp2-cKO^{ob} (Fig. 3B). Decreased expression of *Col1a1* and *Osterix* mRNA was first noted as early as 5 days, and the difference in expression between control and Bmp2-cKO^{ob} progressed with age

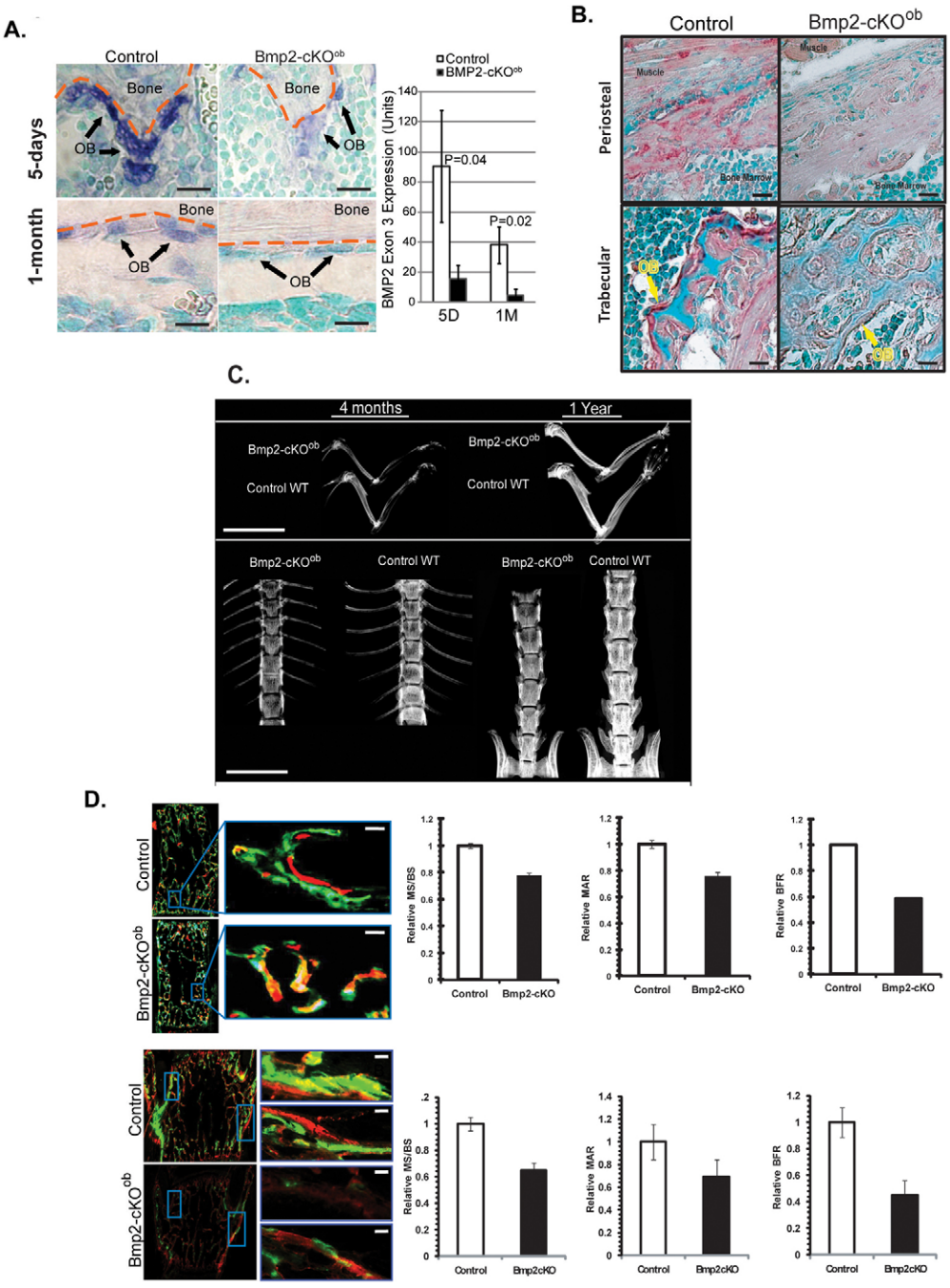

Fig. 1. Osteoblast-selective *Bmp2* deletion in periosteum and trabecular region. (A) *In situ* hybridization (blue) of femurs at 5 days and 1 month. OB, osteoblast. Two independent litters at each age, 2–3 sections and 2–3 photographs per section from femurs were evaluated. (B) Immunocytochemistry of Bmp2 protein expression. OB, osteoblasts on bone surface. Femurs from two independent litters at 1 month of age were evaluated with 2–3 sections with multiple images per section. (C) Radiograph of arms and lower spine at 4 months and 1 year of control and Bmp2-cKO^{ob} mice. Over 200 litters of different ages were evaluated, with a representative X-ray shown. (D) BFR in trabecular region and periosteum in vertebrae from 4-month-old control and Bmp2-cKO^{ob} animals. High-magnification images for trabecular (top) and periosteal (bottom). Two independent litters of control and Bmp2-cKO^{ob} animals were evaluated, and the relative MS/BS and BFR rates are shown. Results are means ± s.d. Scale bars: 20 µm (A,B); 10 mm (C); 40 µm (D).

(supplementary material Fig. S3B). There was a 70% decrease in number of osteoblasts positive for phosphorylated Smad1, Smad5 or Smad8 (p-Smad1/5/8) in bones from Bmp2-cKO^{ob} at 5 days in alveolar bone and at 2 weeks in tibia (supplementary material Fig. S4). In 6-week-old mice, we noted with an anti-phospho-Smad1/5/8 antibody nuclear staining (purple) in osteoblasts of control mice and little cytoplasmic or nuclear localization in the Bmp2-cKO^{ob} (supplementary material Fig. S5, top panels). Also, 20% of the vascular associated cells around small blood vessels (<30 µm), had a robust nuclear (purple to pink) phospho-Smad1/5/8 signal. Little staining of phospho-Smad1/5/8 was observed in the Bmp2-cKO^{ob} blood vessels (supplementary material Fig. S5, middle and bottom panels).

Decreased vascularization and decreased VegfA in the Bmp2-cKO^{ob} mice

Bones of the Bmp2-cKO^{ob} are less red and show reduced blood vessels as assayed with Col IV immunohistochemistry (Fig. 4A). There are reduced levels of CD31 in blood vessels in the Bmp2-cKO^{ob} (supplementary material Fig. S6). We performed vascular perfusion (n=3, control and Bmp2-cKO^{ob}, 7 months) and µCT 3D mapping of the vascular structure in the metaphysis, diaphysis and periosteum of long bones. We used the $BaSO_4$ perfusion method as described in the Materials and Methods (David et al., 2009). We observed a 50% decrease in blood vessels in the diaphysis bone region and a 75% decrease in blood vessel volume per trabecular volume in the Bmp2-cKO^{ob} (Fig. 4B). In the periosteum, we

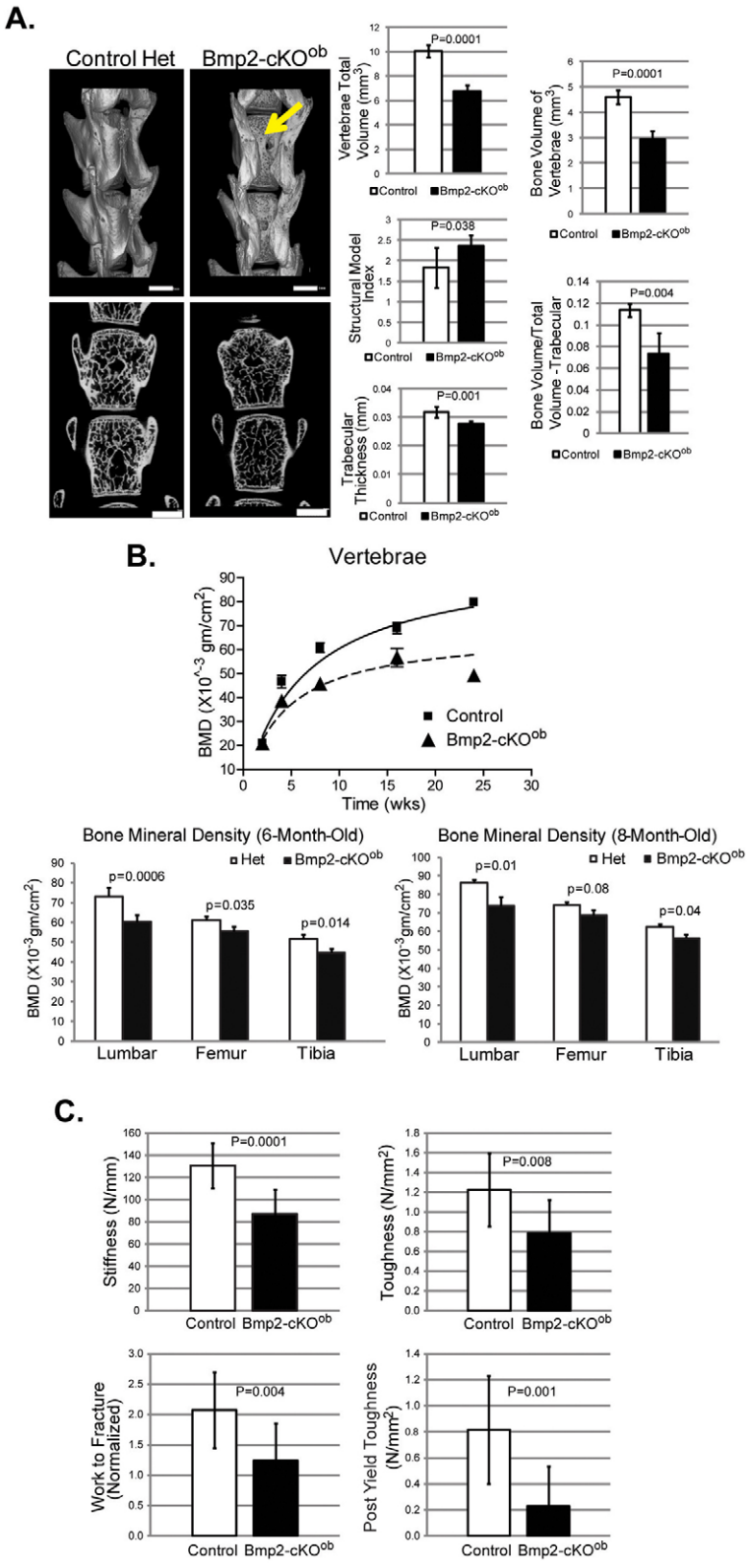

Fig. 2. µCT analysis of vertebrae, BMD analysis of vertebrae and long bones and mechanical testing of femurs from control and Bmp2-cKO^{ob} animals. (A) µCT shows that Bmp2-cKO^{ob} vertebrae have open ventral process (yellow arrow), reduced size and reduced overall bone volume to total volume. Analysis was done with $n=5$ animals of control or Bmp2-cKO^{ob} genotypes. (B) BMD is reduced in Bmp2-cKO^{ob} in both the vertebrae and the long bones, as assayed from 2 weeks to 8 months. Analysis was done on $n=3$–6 animals of the two genotypes at each age. (C) Three-point bending to fracture indicates Bmp2-cKO^{ob} mice have reduced stiffness, work to fracture and dramatically reduced post-yield toughness. Analysis was done on $n=6$–11 mice of each genotype, 4 months of age. Results are means ± s.d. Scale bar: 1 mm.

observed a 75% decrease in blood vessel volume to total volume, a 60% decrease in blood vessel volume to bone surface in the Bmp2-cKO^{ob} and a 75% decrease in blood vessel number per bone surface (Fig. 4C). Blood vessels greater than 20 µm were not affected severely in the Bmp2-cKO^{ob}. However, in the metaphysis, with the many small capillaries and sinusoidal regions in close association with the bone (less than 50 µm away from bone and less than 15 µm in diameter), we observed a marked 90% decrease in these small-bone-associated microvessels in the Bmp2-cKO^{ob} (Fig. 4D, right side). A 3D demonstration of the reduced small

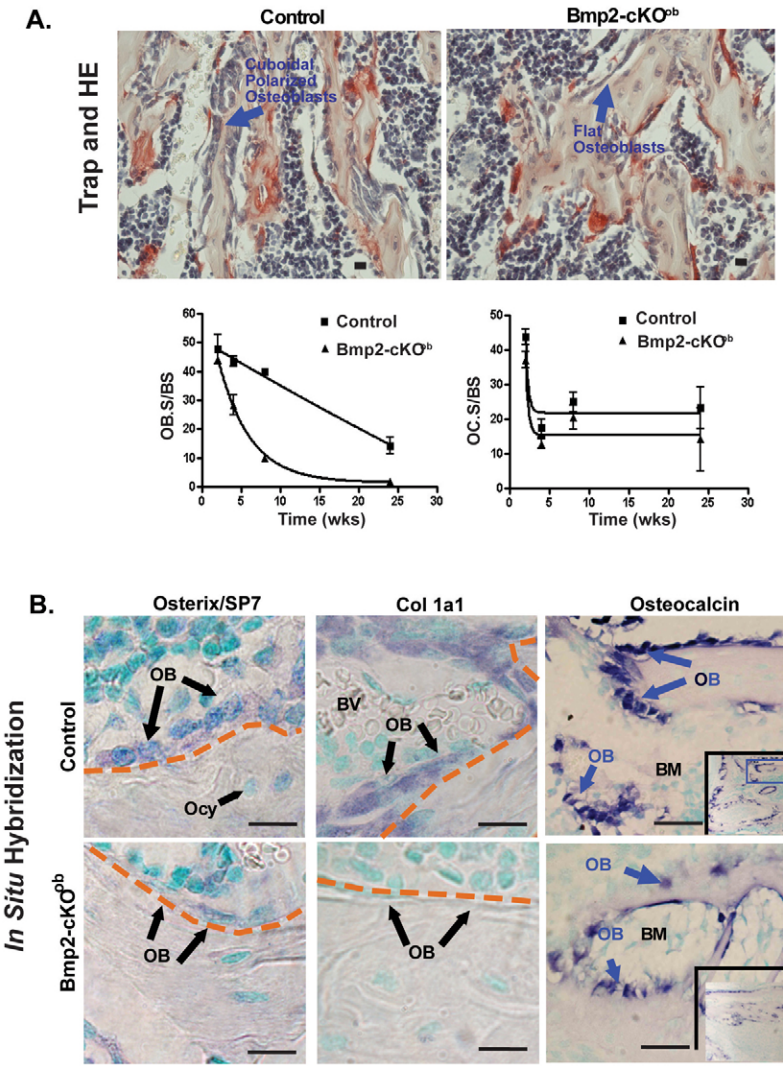

Fig. 3. Histology and histomorphometric analysis and expression of Osterix, Col1a1 and Osteocalcin in control and Bmp2-cKO^{ob}. (A) Histology with Trap staining counterstained with hematoxylin for evaluation of osteoblasts and osteoclasts. Blue arrows indicate osteoblasts. In the Bmp2-cKO^{ob} model, osteoblasts are mostly flat with reduced OB.S/BS (osteoblast surface to bone surface). Three independent litters, with 2–3 sections and 2–3 images of separate regions per section per animal were evaluated for quantified histomorphometric analysis. (B) *Osterix*, *Col1a1* and *Osteocalcin in situ* hybridization in femurs of 5-day-old control and Bmp2-cKO^{ob} animals. Two litters with each genotype, 2–3 sections and 2–3 images of different areas per bone were evaluated. Orange dashed line outlines bone surface; BV, blood vessel; BM, bone marrow; OB, osteoblasts; Ocy, osteocytes. Scale bars: 20 µm.

blood vessels in the Bmp2-cKO^{ob} and close association of blood vessels with the trabecular bone is shown in supplementary material Movie 1. *VegfA* mRNA expression was decreased in Bmp2-cKO^{ob} mice by 60–80% (Fig. 5A). VegfA protein levels in the trabecular region were reduced by ~70% (Fig. 5B).

Expression of marker genes for MSCs *in vivo* are reduced in the Bmp2-cKO^{ob} mice

α-SMA protein (immunoreactivity) was reduced by 60–70% in the Bmp2-cKO^{ob} tibia trabecular region and in the cambial layer of the periosteum (Fig. 6A). CD146 or MCAM was reduced by ~60% in the Bmp2-cKO^{ob} vascular-associated cells next to the endothelial cells (Fig. 6B, top). Reduced numbers of CD146 cells were observed in the periosteum of 5-day-old and 1-month-old Bmp2-cKO^{ob} compared with controls (data not shown).

Using α-SMA-Cherry reporter mice, a 70% reduction in α-SMA^{+} cells per unit of marrow volume was observed in the trabecular region. Confocal analysis on the vascular wall demonstrated a reduced number of α-SMA^{+}–Cherry cells per unit length of blood vessel (Fig. 6B, bottom). Angiopoietin 1 (Ang-1) levels were reduced by 63% in the bone marrow of tibia Bmp2-cKO^{ob} compared with controls, as shown in Fig. 6C. Ang-1 is reported to be important in stable interactions between MSCs and endothelial cells (Carmeliet and Jain, 2011).

MSC population is decreased and presents reduced capacity to differentiate to mature osteoblasts in the Bmp2-cKO^{ob}

There is a 90% reduction in the capacity of clonal bone marrow stromal cells (BMSCs) of Bmp2-cKO^{ob} cells, *in vitro*, to form mineralized matrix (CFU-OB) compared with cultures from heterozygous or wild-type animals, as measured using the methods described in the Materials and Methods (Chen et al., 2007) (Fig. 6D, right). A 70% reduction in the number of CFU-F clones in the Bmp2-cKO^{ob} BMSC cultures, an *in vitro* measure of MSCs, was also noted in the Bmp2-cKO^{ob} (Fig. 6D, left). There was a significant 30% reduction of CFU-F in the Control-Het, suggesting a threshold effect of Bmp2 on MSC clones. rBmp2 (40 ng/ml) added at initial plating to the CFU assay had no effect on the number of CFU-F clones (data not shown).

VegfA activates Bmp2 expression in α-SMA^{+} BMSC cell cultures *in vitro*

Using extracellular matrix, BMSCs maintain their stem cell properties and can be greatly expanded from any BMSC culture.

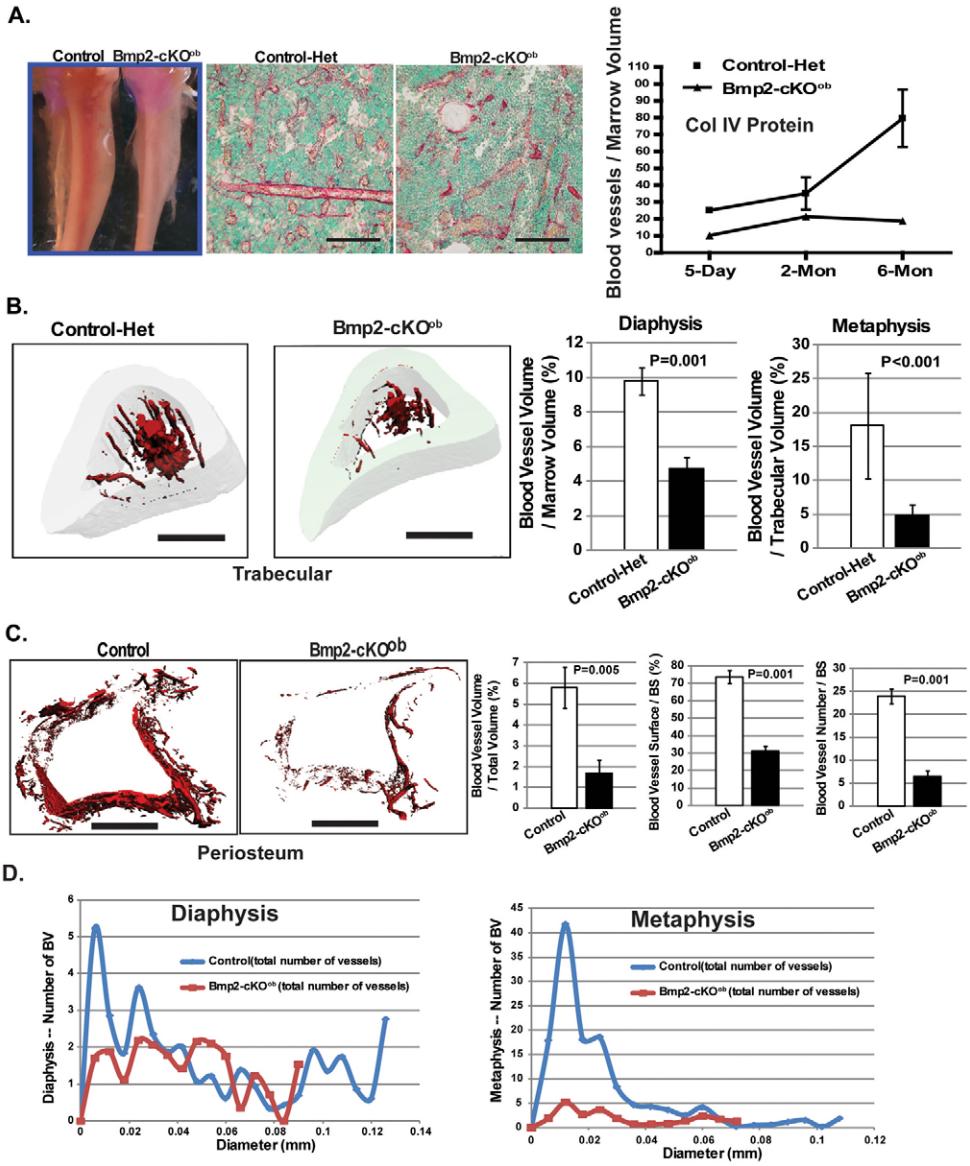

Fig. 4. Vascular defects in the Bmp2-cKO^{ob} model. (A) Tibia of 4-month-old mice and immunostain and quantification of Col1V levels in control and Bmp2-cKO^{ob} animals. One litter was evaluated with 2–3 sections, two different regions per section per tibia at each age. (B) 3D vascularization maps of trabecular blood vessels were made using the method described in the Materials and Methods (David et al., 2009). Blood vessel volume as a function of marrow volume (diaphysis) and BV per trabecular bone volume (metaphysis) were quantified in femurs at 7 months. Three independent litters were evaluated with each genotype. (C) 3D vascular map and quantification of periosteal blood vessels, with reduced blood vessel to total volume, blood vessel surface to bone surface and blood vessel number to bone surface in the Bmp2-cKO^{ob}, in femurs at 7 months. Three independent litters were evaluated for each genotype. (D) Small microvessels (<15 μm in diameter) are dramatically reduced in the metaphysis region of Bmp2-cKO^{ob}, whereas the larger blood vessels are less affected in the metaphysis and diaphyseal region, in femurs at 7 months. Data are the means ± s.d. from the three litters. Scale bars: 100 μm (A); 1 mm (B,C).

BMSCs were grown for 10 days on XC-marrowECM (StemBioSystems LLC, San Antonio, TX). The cells were released with collagenase type 2 and then replated at high density. Over time, we tested the cell response with 100 ng/ml of VegfA. BMSCs grown on the XC-marrowECM were 88% α-SMA positive (α-SMA^{+}) when analysed by FACS (Fig. 7A). VegfA induces *Bmp2* mRNA expression at 4, 24 and 48 hours (Fig. 7A, right). The VegfA induction of *Bmp2* mRNA was validated by qRT-PCR using a TaqMan assay and FAM-labeled primers (data not shown).

α-SMA^{+} BMSCs rapidly differentiate to mature mineral-producing osteoblasts, and the endogenous *Bmp2* gene is required for α-SMA^{+} BMSC differentiation

Supplementary material Fig. S7A shows phase-contrast images (top) and the VonKossa/VanGieson mineral-collagen stain images (bottom) for 7 and 10 day cultures. The α-SMA^{+} BMSCs differentiated into well-organized mineral structures with a characteristic sponge-like or honey-comb appearance of the mineral structures as observed in primary calvarial osteoblasts and in 2T3 osteoblast models (Bonewald et al., 2003; Ghosh-Choudhury et al., 1996). Control cultures form these mineral structures and rBmp2 accelerates osteoblast differentiation and increased minerals, as quantified in supplementary material Fig. S7A. Northern gene expression analysis at day 10 shows high levels of *Osterix*, *Osteocalcin*, *Col1a1* and *Bmp2* expression with increased levels in the rBmp2-treated cultures (supplementary material Fig. S7B).

α-SMA^{+} BMSCs were then cultured and expanded from *Bmp2*$^{fx/fx}$ mice. These cells are 80–90% α-SMA^{+} as determined by FACS, as described above. The α-SMA^{+} cells were treated with either Adenovirus-5 with CMV–GFP (Ad5–GFP) or Adenovirus-5 with CMV–Cre (Ad5–Cre). After 2 days, the cells are collected and replated at high density to be confluent the next day or two. The cultures were changed to differentiation medium (0 day), plus or minus 100 ng/ml rBmp2. Cultures were collected at 1 and 8 days, for gene expression analysis, and at 8 days for evaluation of mineral quality and quantity. As shown in

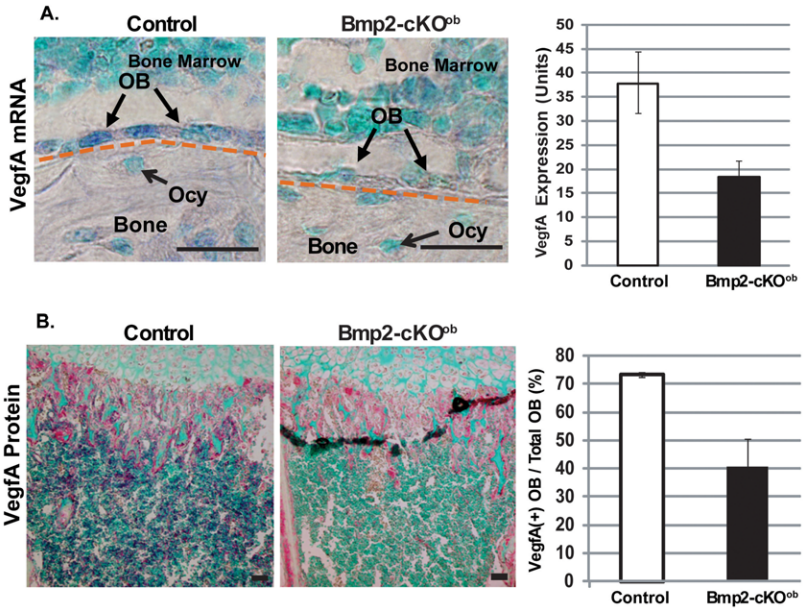

Fig. 5. *VegfA* mRNA and protein expression levels are reduced, as are Angiopoietin 1 protein levels in Bmp2-cKO^{ob} mice. (A) *In situ* hybridization of VegfA expression in osteoblasts of trabecular bone in the femur of 1-month-old control and Bmp2-cKO^{ob} animals. Three independent litters were evaluated with two sections and three images per section per bone with each genotype. Similar results were observed in femurs from 4-month-old animals (data not shown). (B) VegfA protein immunocytochemistry in the trabecular region of the tibia at 5 days of age in control and Bmp2-cKO^{ob} animals. Two independent litters with each genotype were evaluated with average from measurements of 2–3 different sections with multiple images of separate areas per animal. The dark region in the image on the right is an artifact fold in the tissue section. Graphs show means ± s.d. Scale bars: 20 μm (A); 100 μm (B).

Fig. 7B, by dark-field and phase-contrast microscopy, and VonKossa/VanGieson stain, the control cultures (*Bmp2$^{flx/flx}$; Ad5-GFP*) formed well-organized mineral structures as defined above, and rBmp2 accelerated this process. However, in α-SMA^{+} BMSCs in which the *Bmp2* gene is deleted with Ad5–Cre (*Bmp2$^{flx/flx}$; Ad5-Cre*), few mineral structures formed, and importantly, rBmp2 at 100 ng/ml could not rescue this defect in differentiation. Mineral structures were quantified as shown in Fig. 7B. Gene expression analysis of α-SMA^{+} BMSC cultures, with and without the endogenous *Bmp2* gene, was carried out at day 1 and day 8 (Fig. 7C). Expression of the *Bmp2* confirms early reduced Bmp2 levels by day 1, with almost complete loss of *Bmp2* expression at day 8 (Fig. 7C, top left). Osterix expression at day 1 in *Bmp2$^{flx/flx}$; Ad5-GFP* cells was induced fourfold by rBmp2, whereas Cre-treated cells showed little response to rBmp2 (Fig. 7C). Similarly at day 8, Osterix expression continued to increase and was further stimulated by rBmp2 in *Bmp2$^{flx/flx}$; Ad5-GFP* cells, whereas *Bmp2$^{flx/flx}$; Ad5-Cre* cells had reduced Osterix levels in the basal state and showed little response to rBmp2. Basal *Col1a1* expression was reduced in *Bmp2$^{flx/flx}$; Ad5-Cre* cells compared with *Bmp2$^{flx/flx}$; Ad5-GFP* cells at 1 and 8 days. In *Bmp2$^{flx/flx}$; Ad5-Cre* cells at 8 days, there was no rBmp2 increase in *Col1a1* expression compared with the *Bmp2$^{flx/flx}$; Ad5-GFP* cells (Fig. 7C). Similar results were seen with *Osteocalcin* and *Dmp1* gene expression patterns, with *Bmp2$^{flx/flx}$; Ad5-Cre* cells having lost most basal expression as well as displaying a much reduced rBmp2 response. VegfA expression changed little between *Bmp2$^{flx/flx}$; Ad5-GFP* and *Bmp2$^{flx/flx}$; Ad5-Cre* cells at day 1, whether or not they were treated with rBmp2. However, at day 8 there was a threefold increase in VegfA expression in the more mature mineralizing cultures. VegfA expression was slightly higher in control *Bmp2$^{flx/flx}$; Ad5-GFP* cells at 8 days than in Bmp2-treated *Bmp2$^{flx/flx}$; Ad5-GFP* cultures because VegfA levels in the more mature osteoblast–osteocyte cultures were decreasing compared with the less differentiated *Bmp2$^{flx/flx}$; Ad5-GFP* 8 day control cultures (data not shown). However, this late stage (8-day) increase in VegfA expression in *Bmp2$^{flx/flx}$; Ad5-GFP* cells was suppressed in the *Bmp2$^{flx/flx}$; Ad5-Cre* cells, suggesting that differentiation state is a critical component of VegfA levels, and the endogenous *Bmp2* gene is required for this increased VegfA expression. In support of these *in vitro* studies, Bmp2 protein immunoreactivity was frequently associated with the small microvascular walls in the metaphysis region in wild-type mice. However, in the Bmp2-cKO^{ob} mice, vascular-associated Bmp2 protein was greatly reduced (supplementary material Fig. S7C). This suggests that Bmp2 produced by mature osteoblasts induces *Bmp2* expression in the vascular associated MSCs in a paracrine manner because the 3.6Col1a1–Cre is not active in vascular-associated candidate MSCs (supplementary material Fig. S1B).

Discussion

The 3.6Col1a1-cre;Bmp2-cKO^{ob} model deletes *Bmp2* in early osteoblasts and demonstrates a failure of osteoblasts to differentiate to mineralizing state. This was reflected by reduced expression of *Osterix*, *Col1a1* and *Osteocalcin* and by reduced BMP canonical signaling *in vivo*. The bones were much more brittle, as assayed by mechanical testing. We discovered a link between osteoblast terminal differentiation and control of the vascular bed and associated MSCs that is controlled by the osteoblast *Bmp2* gene. We note a massive decrease in micro-capillaries in bone marrow, decreased CD31, CD146, Angiopoietin 1 and α-SMA levels *in vivo* in Bmp2-cKO^{ob} and a decrease in both MSC number and capacity to differentiate with CFU-F and CFU-Ob assays. VegfA levels are reduced in osteoblasts of Bmp2-cKO^{ob} animals and provide a mechanistic link between osteoblasts and angiogenesis and associated MSCs controlled by the *Bmp2* gene. VegfA can activate endogenous Bmp2 production in vascular associated α-SMA^{+} BMSCs *in vitro*. The proposed mechanism is through activation of the Akt–β-catenin pathway (Maes et al., 2010a) because β-catenin can directly activate transcription of *Bmp2* through a TCF–β-catenin response region in the *Bmp2* promoter and the Akt pathway has been shown to activate *Bmp2* transcription (Ghosh-Choudhury et al., 2002; Zhang et al., 2013).

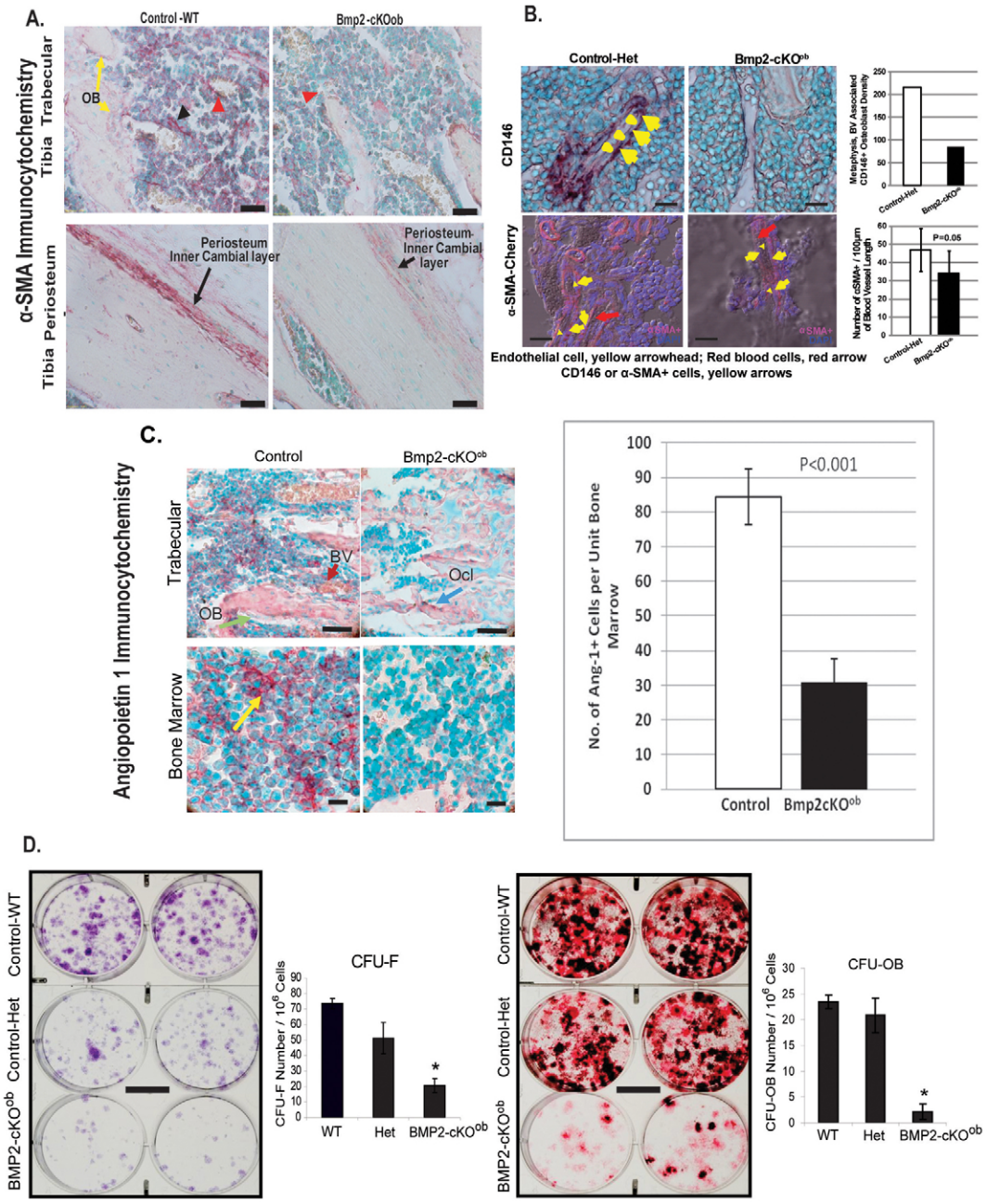

Fig. 6. α-SMA, CD146 and Angiopoietin-1 immunocytochemistry and CFU-F and CFU-Ob assays *in vitro* from control, heterozygous and Bmp2-cKO^{ob} animals. (A) α-SMA immunoreactivity in tibia sections from 1.5-month-old control WT and Bmp2-cKO^{ob} animals. Trabecular region, top; periosteal region, bottom. Yellow arrow with OB indicates low levels of α-SMA. α-SMA decreases as osteoblasts mature (Kalajzic et al., 2008). Black arrowhead indicates dendritic α-SMA^{+} cells not associated with blood vessels; red arrowhead, vascular-associated cells that are α-SMA^{+}. Two independent litters and three sections per bone were evaluated. (B) CD146 protein levels and α-SMA–Cherry reporter levels in control and Bmp2-cKO^{ob} tibia region at 1 month with estimation of signal by ImageJ analysis. Yellow arrowhead indicates endothelial cell. Red arrow, red blood cells. Yellow arrows, CD146^{+} or αSMA^{+} cells. Three independent litters with 3–5 sections per animal were evaluated. (C) Angiopoietin 1 immunocytochemistry is shown in trabecular region of the tibia (top) and the bone marrow (bottom) at 1 month of age and estimation of number of red cells per unit area in 1-month-old control and Bmp2-cKO^{ob} animals. Two litters with each genotype and 2–3 sections per bone were evaluated. Yellow arrow indicates Ang1^{+} cells in bone marrow. (D) CFU-F clonal levels (left) and CFU-OB levels (right) from BMSC cultures from Control-WT, Control-Het and Bmp2-cKO^{ob} 4-month-old animals, n=3. The entire assay was repeated twice with similar results, and a representative experiment is shown. Graphs show means ± s.d. Scale bars: 50 μm (A); 30 μm (B); 50 μm (C, top); 20 μm (C, bottom); 1 cm (D).

Recent findings (Liu et al., 2012) support the idea that VegfA can also drive commitment of osteoblast precursors to mature osteoblasts, and suggest that VegfA acts in part by unknown intracrine mechanisms. VegfA overexpression in bone marrow leads to new bone formation as well as massive angiogenesis (Maes et al., 2010b). We suggest that there is a synergistic interaction of VegfA^{ob} and Bmp2^{ob} coming from mature osteoblasts that is driving new blood vessel formation and

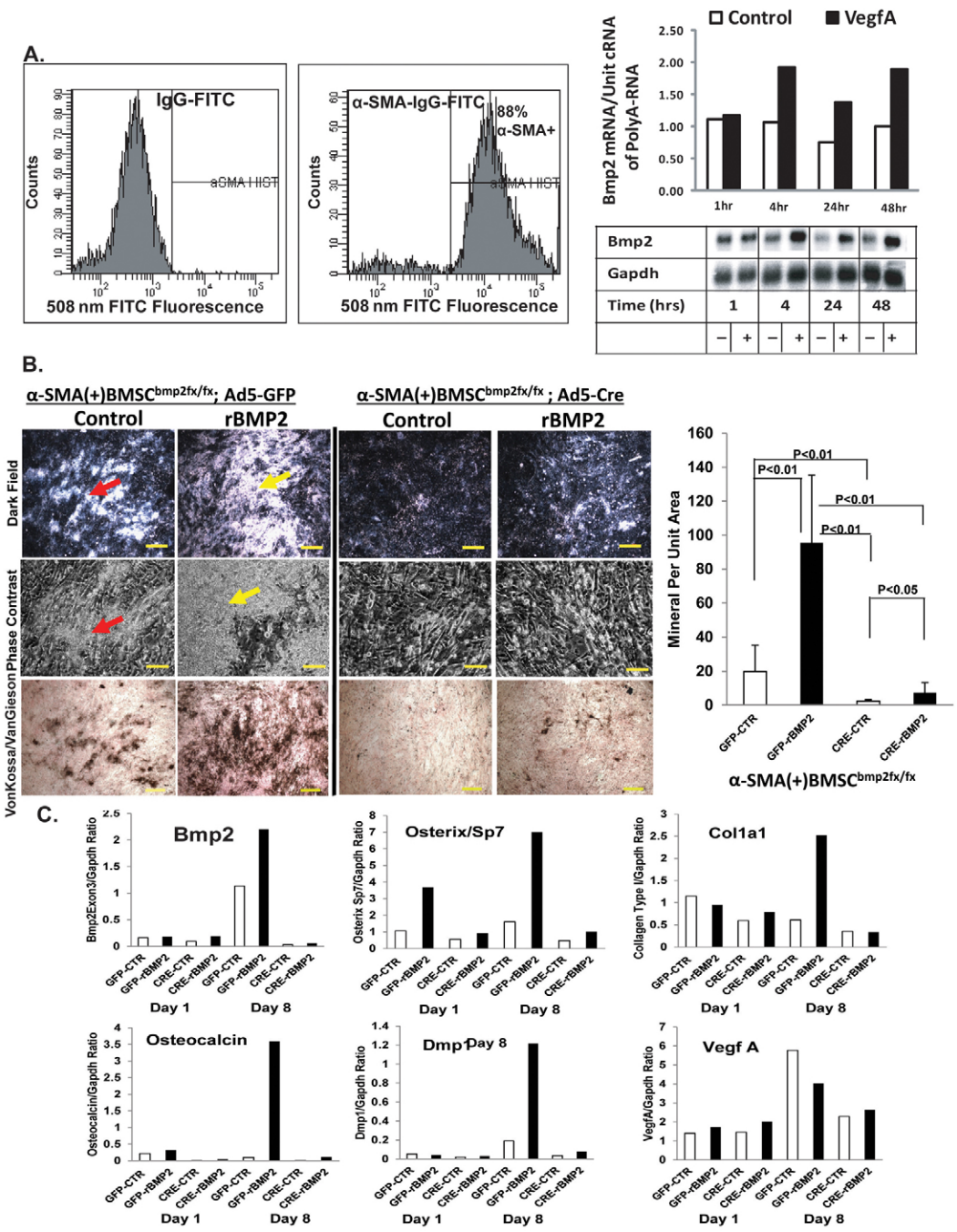

Fig. 7. Enriched α-SMA$^+$ BMSC response to VegfA and requirement of the endogenous *Bmp2* gene in these stem cells for differentiation to mineralizing osteoblasts. (A) FACS analysis of BMSCs expanded on XC-marrowECM with control IgG–FITC on the left, and α-SMA IgG–FITC in the middle. Right panel is northern analysis of *Bmp2* expression of amplified polyA RNA from α-SMA$^+$ BMSCs treated with 100 ng/ml VegfA. (B) Mineral structures without and with 100 ng/ml rBmp2. Dark-field (top), phase-contrast (middle) and VonKossa/VanGieson staining (bottom) of control and rBmp2-treated cultures of α-SMA$^+$ BMSCs infected with either Ad5–GFP or Ad5–Cre before the differentiation assay. Red arrows, control-mineral structures. Yellow arrow, rBMP2-treated mineral structures. Right, quantification of mineralized structures (ImageJ) from two independent cultures with measurements of six to eight 40× fields per well. Scale bars: 100 µm (top and bottom); 20 µm (middle). (C) Northern analysis of *Bmp2*, *Osterix*/*Sp7*, *Col1a1*, *Osteocalcin*, *Dmp1* and *VegfA* mRNA in amplified polyA RNA from 1 and 8 day cultures, with and without rBmp2, in α-SMA$^+$ BMSCs previously treated with either Ad5–GFP or Ad5–Cre. Northern analysis shown is from one representative experiment and experiments were repeated three times with α-SMA$^+$ BMSC *Bmp2*$^{fx/fx}$ cell system for mineralization assays and twice for northern gene expression analysis.

Bmp2^{ob} is activating *Osterix*, *Col1a1*, *VegfA* and *Bmp2* in MSCs. Osterix is known to directly activate many osteoblast differentiation genes, such as *Col1a1* and *VegfA* (Tang et al., 2012), and rBmp2 is known to auto-regulate endogenous Bmp2 expression (Ghosh-Choudhury et al., 1996; Ghosh-Choudhury et al., 2001; Zhao et al., 2002). VegfA plays an intracrine role in driving the MSCs towards the osteoblast lineage (Liu et al., 2012).

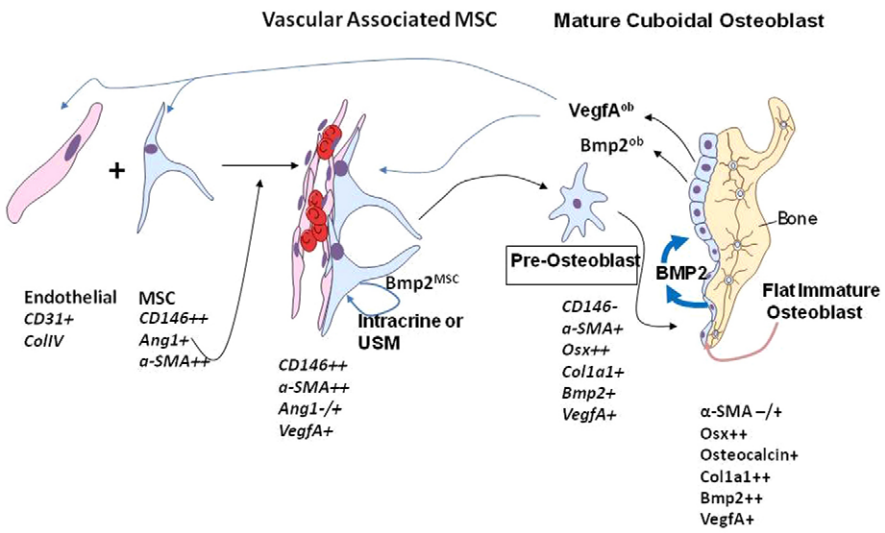

Fig. 8. Model describing the relationship of osteoblast-produced Bmp2 and connections to VegfA production and increased microvascularization that serves as a major niche for mesenchymal stem cells. Bmp2 from osteoblasts ($Bmp2^{ob}$) in an autocrine or cell autonomous manner stimulates osteoblasts to differentiate, produce $VegfA^{ob}$ and increase $Bmp2^{ob}$ protein. $VegfA^{ob}$ in combination with Angiopoietin 1 stimulates new stable microvascular structures with associated vascular MSCs. $Bmp2^{ob}$ stimulates Bmp2 expression ($Bmp2^{msc}$) in a paracrine manner in the associated MSCs leading them to differentiate into mature osteoblasts. Endothelial cells could be a source for *Bmp2* expression induced by Bmp2 and other BMPs in the bone marrow environment and that increased BMP signaling in endothelial cells or endothelial cell precursors could contribute in a physiological manner to new MSCs through mechanisms similar to that observed in heterotopic ossification pathologies (Medici and Olsen, 2012). Primarily, we propose that $Bmp2^{ob}$ stimulates endogenous $Bmp2^{msc}$, which collectively drives the MSC to osteoblast differentiation pathway in an intracrine or unconventional secretory mechanism (USM) pathway. VegfA contributes to this lineage commitment of the MSCs into mature osteoblasts (Liu et al., 2012).

A model is presented in Fig. 8 in which osteoblast Bmp2 ($Bmp2^{ob}$) induces VegfA from osteoblasts ($VegfA^{ob}$) stimulates new vascularization and microvessels (capillaries) with associated MSCs. Angiopoietin 1 plays a key role in integration and stabilization of the MSCs with the vascular–endothelial structures (Carmeliet and Jain, 2011). $VegfA^{ob}$ and $Bmp2^{ob}$ from osteoblasts, in turn, activate endogenous *Bmp2* expression in these vascular-associated MSCs ($Bmp2^{msc}$). The endogenous $Bmp2^{msc}$ once activated, is then required for progression of the MSCs to osteoblasts and appears to function in some unknown intracrine manner that might allow endogenous Bmp2 to accumulate locally on the plasma membrane, possibly by unconventional secretion mechanisms (USMs) (Nickel, 2003; Askarinam et al., 2013). Bmp2 from osteoblasts could also drive endothelial cells to undergo an endothelial mesenchymal transformation (EndoMT), as happens in pathological heterotopic ossification (HO), and these progenitors cells could then contribute to skeletal ossification as well (Medici et al., 2010; Medici and Olsen, 2012; Lounev et al., 2009).

Our data also suggest that greatly reduced collagen production in the bone matrix in the absence of Bmp2 in osteoblasts leads to bones of poor quality and increased brittleness (Burr, 2002). The combined effects of failure of late stage osteoblast differentiation, leading to poor bone quality, is linked to defects in formation of microvessels closely associated with new bone formation and the home of at least one class of MSC required for formation of bone.

The link between Bmp2 and angiogenesis is, first, supported by elevated generalized BMP signaling in osteoblasts to increase VegfA production and increase bone and blood vessels (Zhang et al., 2009). Second, during distraction osteogenesis, *Bmp2* expression is induced in the vascular-associated cells (candidate MSCs) and possibly in the endothelial cells as well (Matsubara et al., 2012). Third, antibody blockage of VegfR1 and VegfR2 leads to much reduced numbers of blood vessels, reduced new bone formation and reduced *Bmp2* expression in the distraction osteogenesis model (Jacobsen et al., 2008). Fourth, conditional removal of VegfA in osteoblast precursors ($Osterix^{+}$) leads to greatly reduced bone formation (Liu et al., 2012). Fifth, mechanical-load-induced new bone in the mouse ulna causes an increase in Bmp2 and VegfA expression in vascular associated cells in the periosteum within 1 day (Martinez et al., 2010). Emerging evidence suggests that at least one location for the MSC niche is on the microvessels, and these perivascular-associated MSCs express high levels of α-SMA and CD146 (Sacchetti et al., 2007). Mouse $\alpha\text{-SMA}^{+}$ vascular-associated cells show properties of MSCs by lineage tracing studies (Grcevic et al., 2012). These $\alpha\text{-SMA}^{+}$ cells, isolated from fat tissue, when placed in an irradiated mouse, can reconstitute the bone marrow and bone and differentiate into osteoblasts (Kalajzic et al., 2008). Our data, at least *in vitro*, show that $\alpha\text{-SMA}^{+}$ BMSC cultures require the endogenous *Bmp2* gene to progress to differentiated osteoblasts.

The periosteum of bone controls periosteal bone expansion and is critical for determining bone size and is also an important target for mechanical loading (Allen et al., 2004; Bandyopadhyay et al., 2008). Fatigue loading of bone can induce *Bmp2* expression in vascular-associated cells in periosteum (Wohl et al., 2009). Bmp2, specifically in periosteal progenitors, plays a key role in bone healing (Wang et al., 2011). The major phenotype in $Bmp2\text{-cKO}^{ob}$ and in the Prx1–Cre Bmp2 model (Tsuji et al., 2006) is long bones that are all much thinner in

cross-sectional diameter, supporting a major role in periosteal function. α-SMA^{+} cells in the periosteum are greatly reduced in the Bmp2-cKO^{ob} model.

In summary, we demonstrate that the *Bmp2* gene in osteoblasts is required in terminal differentiation and proper mineral-matrix formation, in both periosteum and trabecular bone. Ablation of Bmp2 leads to poor quality bone. We also provide evidence that terminal differentiation, driven by Bmp2 in osteoblasts, is linked to angiogenesis and MSCs by both VegfA level and endogenous Bmp2 protein in MSCs. The phenotype of the Bmp2-cKO^{ob} model in several aspects mimics what happens to bone during aging in mice and humans, such as reduced vascularization and associated MSCs and decreased osteoblast number and differentiation.

Materials and Methods

Generation of the Bmp2-cKO^{ob} mice using 3.6Col1a1-Cre

All animal experiments were performed according to approved guidelines. Details of production of the *Bmp2*^{fx} model are given in supplementary material Fig. S1A. A 5.0 kb *Kpn*I-*Acc*III 5′ fragment and a 4.5 kb *Acc*III-*Sal*I 3′ fragment were used. A polII-neo cassette flanked by FRT sites and *loxP* site, a splicing acceptor site that splices a human alkaline phosphatase expression cassette (Moon et al., 2000) in-frame with coding exon 2, was introduced into an *Acc*III site in the 3′ untranslated region of exon 3. A 5′ *loxP* site marked by a *Pst*I site was placed at *Xho*I site in intron 2. Mice heterozygous for *Bmp2* floxed allele with a polII-neo cassette (fn/+, fx with neo cassette) were bred with C57BL/6 Flipper mice containing a β-actin promoter driving flip recombinase (Jackson Labs) to remove the neo cassette (fx/+). The fn/+ (fn is the *Bmp2* floxed allele with the neo cassette before removal by the flip recombinase, and both exon 3 and neo cassette are removed at the same time by Meox2-Cre) mice were also bred with Meox2-Cre mice (Jackson Labs) to delete exon 3 and neo cassette and generate recombined null allele. Bmp2 Rec/+ is the same as *Bmp2*$^{fx/+}$ after recombination with Cre from the *Meox2* promoter.

Genotypes were determined by Southern blots with 5′ and 3′ external probes (supplementary material Fig. S1A, bottom left). For PCR analyses, primers A and B were used to amplify fragments from wild type (262 bp) and *Bmp2* floxed alleles (362 bp for both fn and fx). Primers A and C were used to detect null allele (367 bp) generated by Zhang and Bradley (Zhang and Bradley, 1996). Primers D and F were used to detect flip-dependent deletion of the neo cassette (450 bp for fx, 194 bp for wild type with primers D and E), and primers A and F were used to detect Cre-dependent deletion of the floxed region (450 bp for Rec=Bmp2 floxed allele after Cre recombination) (supplementary material Fig. S1A, bottom right). Primers: A (5′-AGCATGAACCCTCATGTGTTGC-3′); B (5′-CTCGTATC-CATCTCATCCTCATTCG-3′); C (5′-GAGACTAGTGAGACGTGCTACT-3′); D (5′-AGGGTTTCAGGTCAGTTTCCG-3′); E (5′-TCCGAAGGTAAGTGTG-CTTGG-3′); F (5′-GATGATGAGGTTCTTGGCGG-3′); G (5′-AATGGTTTG-TCCTACGCATCG-3′).

Functional test of *Bmp2* floxed allele

Bmp2 null (B2KO is the *Bmp2* allele with complete exon 3 deletion globally) heterozygotes were crossed with themselves and wild-type, B2KO/+ and B2KO/KO embryos were evaluated around 8–9 d.p.c. Intercrosses between mice heterozygous for B2Rec (*Bmp2* floxed allele recombined after Cre event)/+ were also set up to obtain wild-type, B2Rec/+ (*Bmp2*^{fx}-recombined/+=*Bmp2* Hets) and B2Rec/Rec (*Bmp2*^{fx}-recombined/Bmp2^{fx}-recombined=*Bmp2* null) embryos, using the MeoxCre mice that delete in the blastocyst. The recombined fx allele (B2Rec) was confirmed with primers A+F. B2KO (*Bmp2* allele with permanent global removal of *Bmp2* gene)/+ mice for *Bmp2* were crossed with B2Rec/+ mice to obtain B2Rec/KO embryos and to compare their morphology with B2KO/KO (standard global *Bmp2* KO embryo) and B2Rec/B2Rec (Bmp2-KO$^{Meox2\text{-}Cre}$) embryos. Data are shown in supplementary material Fig. S1A, far right. These results demonstrate that our *Bmp2*^{fx} allele, without the neo cassette, is totally functional since deletion of both *Bmp2*^{fx} alleles in homozygous state (Bmp2-KO$^{Meox2\text{-}Cre}$) at the blastocyst stage gives the same phenotype as the global *Bmp2* KO animals, with failure to form a heart or amnionic structures (Zhang and Bradley, 1996).

Specificity of the 3.6Col1a1-Cre line by crossing to the Rosa26-*loxP*-*lacZ*-*loxP*-td-Tomato

Only the 3.6Col1a1-Cre allele from the male germline was used for mouse crosses to assure specificity and selectivity (Liu et al., 2004). However, the 3.6Col1a1-Cre is active in a variety of cells expressing type 1 collagen in the embryo but at much lower levels than after birth, when bone formation and Col1a1 expression greatly increases. Deletion of the *Bmp2* gene in these embryonic tissues apparently has a minor bone phenotype, as shown in supplementary material Fig. S2. Another possibility is that during embryogenesis, maternal-derived Bmp2 'rescues' these potential phenotypes, as we have shown in global partial Bmp2 KO (when we have the neo cassette in the *Bmp2* gene=*Bmp2*^{fn}/*Bmp2*^{fn}); however, there is rescue of the *Bmp2* hypomorphic embryonic defects if the mother has one WT allele (Singh et al., 2008).

The bone-specific expression postnatally with the 3.6Col1a1-Cre model was validated by crossing with Rosa26-*loxP*-stop-*loxP*-td-Tomato allele in which the tdTomato reporter (orange-red) expresses when a Cre event occurs [B6.Cg-Gt(Rosa)26Sortm9(CAG-tdTomato)Hze/J]. As shown in supplementary material Fig. S1B, we observed the 3.6Col1a1-Cre (orange-red Tomato+ cells) activity predominantly expressed in the bone-associated osteoblasts at 1 month of age. There are a few dendritic cells in the diaphyseal marrow region that resemble preosteoblasts, as previously described in the 3.6Col1a1–GFP model (Kalajzic et al., 2008). We observed strong Cre activity in several layers of the periosteum and associated tendons (supplementary material Fig. S1B, right). No Cre activity was detected in the vast majority of the bone marrow nor in the muscle or growth plate chondrocytes and importantly, not in or around the blood vessel sinusoidal regions of the metaphysis.

We then crossed *Bmp2* floxed allele with 3.6Col1a1-Cre mice to generate the 3.6Col1a1-Cre;Bmp2fx/Bmp2fx or 3.6Col1a1-Cre;Bmp2fx/Bmp2KO, referred to as Bmp2-cKO^{ob}, to selectively delete the *Bmp2* gene in preosteoblasts.

Alizarin Red and Alcian Blue staining

Mice were sacrificed for Alizarin Red and Alcian Blue staining to evaluate ossified tissue and cartilage respectively, at birth and 2 weeks of age, as described (McLeod, 1980).

Histology and histomorphometric evaluation

Bone tissues were collected from Bmp2-cKO^{ob} and their littermate controls at the regions of vertebrae, femur, tibia and mandible. Bones from the left side were prepared for radiology study, and the right bones were prepared for bone histological evaluation. Bone samples were fixed in RNase-free 4% paraformaldehyde, demineralized in RNase-free 15% EDTA for 6 weeks at 4℃ and embedded in paraffin. 8 μm sections were then prepared for Hematoxylin and Eosin (HE) with Orange E, tartrate-resistant acid phosphatase (TRAP) staining, immunohistochemistry and *in situ* hybridization. Bone samples were fixed in 70% ethanol for 3 days followed by plastic resin embedding without demineralization and sections cut at 8 μm. Bone histomorphometric analysis was carried out on the HE- and TRAP-stained samples using Bioquant (www.bioquant.com). At least two different litters at each age, and their appropriate littermates, were evaluated for most parameters, with multiple sections and photographs of each section for each test, as described in detail in each figure legend.

Radiography, bone densitometry and quantification μCT

Male mice aged 2 weeks, 1, 2, 4, 6 and 8 months and 1 year, from over 200 litters, were evaluated by X-ray. Bone samples were processed and stored in 70% ethanol for high resolution X-rays or μCT of individual bones. Digital X-ray images were captured using Faxitron radiographic inspection unit (Model 8050-020, Field Emission Corporation). Bone mineral density (BMD) was evaluated using GE Lunar PIXImus II densitometer. Quantification μCT analysis was carried out for vertebrae and long bones, using a μCT40 Scanco Medical, Zurich, Switzerland (10 μm isometric voxel resolution at 200 msecond exposure, 2000 views and 5 frames per view).

Dynamic bone formation rate

Fluorochrome labeling agents Calcein Green (5 mg/kg) and Alizarin Red (20 mg/kg) were injected peritoneally with a 7-day interval in 1-month-old and 4-month-old male mice. The mice were sacrificed and tissues were collected 3 days after the second injection, followed by the preparation procedure for plastic sectioning as described above. Utilizing Bioquant, MS/BS and MAR were measured and the BFR was then calculated in both the periosteum and trabecular bones using both vertebrae and femurs.

Geometric evaluation and biomechanical tests

Each femur was placed on lower support points of a three point bending fixture with anterior side down. The span (L) between the lower supports was 8 mm. Next, the hydrated bone was loaded-to-failure at 3.0 mm/minute (DynaMight 8841, Instron, Canton, OH) to generate a force versus displacement (P–d) curve. Mechanical and structural properties, and implied material properties have been determined and defined (Nyman et al., 2011).

In situ hybridization

Digoxigenin-labeled complementary RNA probes were transcribed from linearized plasmids that encode *Bmp2* exon 3, *Col1a1*, *Osterix*, *Osteocalcin*, *Dmp1*, *VegfA* and *CD146* mouse cDNAs. *In situ* hybridization was performed following the method previously described (Gluhak-Heinrich et al., 2008; Yang et al., 2012).

Probe concentrations were determined to be in the linear range by dot-blot analysis. Numerical estimation was obtained by ImageJ quantification of the blue digoxigenin–antibody complex (Gluhak-Heinrich et al., 2010; Yang et al., 2012). Two independent littermates at a given age were used with 2–3 sections, with multiple photographs, evaluated from each animal and each probe.

Immunohistochemistry

Immunohistochemistry was performed as previously described (Gluhak-Heinrich et al., 2010; Yang et al., 2012). The red reactive substrate for alkaline phosphatase on the secondary anti-rabbit IgG antibody was quantified by ImageJ with the appropriate no primary antibody controls as described in detail (Yang et al., 2012; Gluhak-Heinrich et al., 2010). Rabbit anti-mouse Osterix Ab22552 (1:50), Rabbit anti-mouse Collagen-IV Ab6586 (1:500), Rabbit anti-mouse Vegf Ab46154 (1:200), Rabbit anti-mouse CD146 Ab75769 (1:200) and Bmp2 antibody Ab14933 were obtained from Abcam Limited (Boston, MA). The phospho-Smad1/5/8 antibody was from Cell Signaling Technology (#9511). The relative capillary density was estimated by the number of capillaries multiplied by the average length of capillaries in the defined area, with the ColIV data. The α-SMA antibody Ab5694 (1:200) and the CD31 antibody Ab28364 (1:50) were also obtained from Abcam.

Isolation of primary bone marrow stromal cells and enrichment of α-SMA$^+$ cells

BMSCs were collected from the femurs and tibias of 3- to 4-month-old wild-type or *Bmp2*$^{fx/fx}$ mice, followed by centrifugation at 1000 r.p.m. at room temperature and then resuspended in Hanks' Balanced salt solution. Cell debris was removed by filtration. Eagle's MEM with Hanks' salts, penicillin (100 U/l), streptomycin (0.1 mg/l) and L-glutamine (PSG) (2 mM) supplemented with 15% FBS was used for BMSC cultures. The BMSCs were expanded on a special extracellular matrix (XC-marrowECM, StemBioSystems) for 10 days, which maintains mesenchymal stem cell properties. Loose and non-adherent cells were removed and cells were then washed twice with PBS and removed with collagenase (Worthington, Type 2, CLS2, 340 U/mg) digestions as described (Chen et al., 2007). From the long bones (femur and tibia) of five mice, we generated over 40–50 million α-SMA$^+$ BMSC cells, WT or *Bmp2*$^{fx/fx}$. The cells were plated in six-well plates on plastic at 500,000 cells per well and tested for VegfA regulation of *Bmp2* expression in 0.05% FCS.

VegfA and rBmp2 treatment of BMSCs enriched for α-SMA$^+$ cells

α-SMA$^+$ levels were determined using mouse monoclonal IgG antibody to α-SMA-conjugated to FITC (Sigma, Clone 1A4). Appropriate mouse IgG–FITC was used as a control. Sample-test cells for FACS analysis were first permeabilized with 0.01% Triton X-100 on ice for 10 minutes before adding antibodies. FACS analysis was carried out with the BD Aria FACS analysis instrument (BD Biosciences). The BMSC α-SMA$^+$ cells (>80% α-SMA$^+$) were placed in 0.05% FCS for 24 hours and then VegfA was added at 100 ng/ml for 4, 24 and 48 hours and *Bmp2* expression levels were determined by northern analysis and qRT-PCR using 18S ribosomal as control and TaqMan assay, Applied Biosystem FAM label primers (Rn 18S, Mm03928990 and mBmp2, Mm01340178). Long-term cultures of α-SMA$^+$ BMSCs were carried out in 15% FCS αMEM, 50 μM ascorbic acid and 5 mM beta-glycerol-phosphate (differentiation medium), plus and minus rBmp2 at 100 ng/ml. The cultures were stopped at 7 and 10 days to evaluate mineral-matrix production using VonKossa and VanGieson stains (Ghosh-Choudhury et al., 1996), phase-contrast microscopy for mineral and collagen matrix and subsequently RNA extraction and amplification of polyA RNA to ds cDNA and then cRNA, for northern analysis. Von Kossa staining was evaluated and quantified from low magnification (40×) photographs taken under constant setting brightfield illumination. Six independent areas per well, in duplicate wells per test-time were quantified for 'black' regions using a constant threshold (dependent on illumination setting of photographs) setting using ImageJ software.

In some experiments, BMSC preparations with the XC-ECM were prepared with bone marrow from *Bmp2*$^{fx/fx}$ animals. The cells were again tested for α-SMA by FACS and were over 85% positive. These α-SMA$^+$ BMSC$^{bmp2fx/fx}$ cells were then set up at 50% confluence in 10 cm plates in 2% FCS α-MEM and infected with either Ad5-CMV-GFP or Ad5-CMV-Cre at 10,000 particles per cell (Virus Development Laboratory, Baylor College of Medicine, Houston, TX). After 2 days, over 90% of the GFP-infected cells were GFP$^+$. The cells were trypsinized and replated on six-well rat-tail-collagen-coated (1 to 10 dilution of BD Biosciences rat tail collagen in water, for 30 minutes, followed by air drying) plates at 700,000 cells per well and allowed to reach confluence, changed to differentiation medium, plus or minus rBmp2 at 100 ng/ml. Medium was changed every 2–3 days. Samples were stopped at 8 days (most dynamic range for differentiation) for evaluation of mineral structures by VonKossa, VanGieson, phase and dark-field microscopy and stopped at day 1 and day 8 for RNA extraction, amplified polyA RNA to ds cDNA and cRNA, northern analysis using *Bmp2* exon 3 probe and full-length coding cDNAs for *Osterix*, *Col1a1*, *Osteocalcin*, *Dmp1* and *VegfA* probes.

CFU-F and CFU-OB assays

The freshly isolated BMSCs were expanded and prepared for CFU assays at clonal densities, as previously described (Chen et al., 2007), using 4-month-old control WT, control Het and Bmp2-cKO^{ob} mice. After 2 weeks of culture, CFU-F colonies were evaluated using Crystal Violet staining. CFU-OB colonies were evaluated by VonKossa staining after osteogenic induction with the addition of 50 μM ascorbic-acid-2-phosphate, 10 mM β-glycerophosphate and 100 mM dexamethasone. CFU colony assays with or without 40 ng/ml rBmp2 was also performed.

α-SMA-Cherry transgenic mice

An α-SMA1–Cherry reporter transgenic model was used to monitor vascular associated MSCs *in vivo*. The transgene consisted of a 2 kb α-SMA (*Acta1* gene) promoter region linked to the Cherry reporter cDNA (Grcevic et al., 2012). The bone tissues from 1- and 2-month old α-SMA-Cherry;Bmp2cKO^{ob} and their littermates, α-SMA-Cherry;Bmp2Het or α-SMA-Cherry;WT, were collected and fixed with 4% paraformaldehyde at 4°C for 1–2 days, followed by demineralization in 15% EDTA (changed every day) for 7–10 days and then placed in 30% sucrose until ready to embed. Tissues were embedded in OCT-Tissue-Tek #4583 (Electron Microscopy Sciences, Hatfield, PA) and sectioned at 8 μm thickness, using the Kawamoto tape system for preservation of bone tissue morphology. The α-SMA$^+$ population *in vivo* was then observed after DAPI staining on the tissue-tape using a confocal Olympus FV 1000 microscope. The visualized images were analyzed using a FV10-ASW 2.1 Viewer (Olympus) and reconstruction of stacks was created with the AutoVisualize component of AutoQuant (Media Cybernetics, Bethesda, MD).

Vascular μCT and 3D blood vessel mapping

3D vascularization of periosteal and bone marrow regions was carried out using the $BaSO_4$ method that allows detailed visualization of the microvascular structures in bone marrow and on the periosteum at 2–5 μm resolution (David et al., 2009). Vascularization was assessed with a threshold of 200, whereas bone was at a threshold of 600 by μCT. The vascular maps were independently isolated for the metaphysis region, a volume just below the growth plate that includes the trabecular bone and a volume in the diaphysis region, near the middle of the bone shaft of the femurs and tibias that were analyzed. The periosteal vascular region was carried out in a similar manner, near the metaphysis region. The diameter of the blood vessels were then binned into different size classes and plotted as total blood vessels within a given diameter range.

Statistical analysis

Student's *t*-tests and ANOVA were performed to compare data between Bmp2-cKO^{ob} and their littermate wild-type and heterozygous mice using GraphPad Prism software and Microsoft Excel. $P<0.05$ was considered as statistical significance. For immunocytochemistry and *in situ* hybridization, at least two independent litters were evaluated for each probe or antibody with two to three sections, with multiple photographs per section from a given animal. All error bars in the figures represent the s.d.

Acknowledgements

We thank NIEHS for allowing S. E. Harris to work on producing the *Bmp2* floxed mouse model with help of members of Dr Yuji Mishina's lab. This study is dedicated to Gregory R. Mundy.

Author contributions

Study design: S.E.H. Study conduct: W.Y., A.R., J.G.-H., M.A.H., X.-D.C., V.D and S.E.H. Generation and production of Bmp2 floxed mouse models: S.E.H., D.G., G.S., R.M., Y.M. and J.F.M. Assistance with histology, uCT, vascular studies and mechanical testing: J.N., J.R.E., V.D., D.Q. and S.L. Construction and supply of 3.6Col1a1-Cre and a-SMA-Cherry mice: A.L., B.K., D.R. and I.K. Data analysis: M.A.H., J.G.-H., W.Y., S.E.H., J.N. and V.D.

Funding

This work was supported by the US National Institutes of Health [grant numbers R01 AR054616 and AR44728 to S.E.H.; R01DE020843 and ES071003-11 to Y.M.]. Deposited in PMC for release after 12 months.

Supplementary material available online at
http://jcs.biologists.org/lookup/suppl/doi:10.1242/jcs.118596/-/DC1

References

Allen, M. R., Hock, J. M. and Burr, D. B. (2004). Periosteum: biology, regulation, and response to osteoporosis therapies. *Bone* **35**, 1003-1012.

Araldi, E. and Schipani, E. (2010). Hypoxia, HIFs and bone development. *Bone* **47**, 190-196.

Askarinam, A., James, A. W., Zara, J. N., Goyal, R., Corselli, M., Pan, A., Liang, P., Chang, L., Rackohn, T., Stoker, D. et al. (2013). Human perivascular stem cells show enhanced osteogenesis and vasculogenesis with Nel-like molecule I protein. *Tissue Eng. Part A* **19**, 1386-1397.

Bandyopadhyay, A., Tsuji, K., Cox, K., Harfe, B. D., Rosen, V. and Tabin, C. J. (2006). Genetic analysis of the roles of BMP2, BMP4, and BMP7 in limb patterning and skeletogenesis. *PLoS Genet.* **2**, e216.

Bandyopadhyay, A., Kubilus, J. K., Crochiere, M. L., Linsenmayer, T. F. and Tabin, C. J. (2008). Identification of unique molecular subdomains in the perichondrium and periosteum and their role in regulating gene expression in the underlying chondrocytes. *Dev. Biol.* **321**, 162-174.

Bianco, P., Robey, P. G., Saggio, I. and Riminucci, M. (2010). "Mesenchymal" stem cells in human bone marrow (skeletal stem cells): a critical discussion of their nature, identity, and significance in incurable skeletal disease. *Hum. Gene Ther.* **21**, 1057-1066.

Bonewald, L. F., Harris, S. E., Rosser, J., Dallas, M. R., Dallas, S. L., Camacho, N. P., Boyan, B. and Boskey, A. (2003). von Kossa staining alone is not sufficient to confirm that mineralization in vitro represents bone formation. *Calcif. Tissue Int.* **72**, 537-547.

Bonilla-Claudio, M., Wang, J., Bai, Y., Klysik, E., Selever, J. and Martin, J. F. (2012). Bmp signaling regulates a dose-dependent transcriptional program to control facial skeletal development. *Development* **139**, 709-719.

Burr, D. B. (2002). The contribution of the organic matrix to bone's material properties. *Bone* **31**, 8-11.

Carmeliet, P. and Jain, R. K. (2011). Molecular mechanisms and clinical applications of angiogenesis. *Nature* **473**, 298-307.

Chen, X. D., Dusevich, V., Feng, J. Q., Manolagas, S. C. and Jilka, R. L. (2007). Extracellular matrix made by bone marrow cells facilitates expansion of marrow-derived mesenchymal progenitor cells and prevents their differentiation into osteoblasts. *J. Bone Miner. Res.* **22**, 1943-1956.

Crisan, M., Yap, S., Casteilla, L., Chen, C. W., Corselli, M., Park, T. S., Andriolo, G., Sun, B., Zheng, B., Zhang, L. et al. (2008). A perivascular origin for mesenchymal stem cells in multiple human organs. *Cell Stem Cell* **3**, 301-313.

David, V., Martin, A., Hedge, A. M. and Rowe, P. S. (2009). Matrix extracellular phosphoglycoprotein (MEPE) is a new bone renal hormone and vascularization modulator. *Endocrinology* **150**, 4012-4023.

Deckers, M. M. L., van Bezooijen, R. L., van der Horst, G., Hoogendam, J., van Der Bent, C., Papapoulos, S. E. and Löwik, C. W. (2002). Bone morphogenetic proteins stimulate angiogenesis through osteoblast-derived vascular endothelial growth factor A. *Endocrinology* **143**, 1545-1553.

Dutko, J. A. and Mullins, M. C. (2011). SnapShot: BMP signaling in development. *Cell* **145**, 636, e1-e2.

Ghosh-Choudhury, N., Windle, J. J., Koop, B. A., Harris, M. A., Guerrero, D. L., Wozney, J. M., Mundy, G. R. and Harris, S. E. (1996). Immortalized murine osteoblasts derived from BMP 2-T-antigen expressing transgenic mice. *Endocrinology* **137**, 331-339.

Ghosh-Choudhury, N., Choudhury, G. G., Harris, M. A., Wozney, J., Mundy, G. R., Abboud, S. L. and Harris, S. E. (2001). Autoregulation of mouse BMP-2 gene transcription is directed by the proximal promoter element. *Biochem. Biophys. Res. Commun.* **286**, 101-108.

Ghosh-Choudhury, N., Abboud, S. L., Nishimura, R., Celeste, A., Mahimainathan, L. and Choudhury, G. G. (2002). Requirement of BMP-2-induced phosphatidylinositol 3-kinase and Akt serine/threonine kinase in osteoblast differentiation and Smad-dependent BMP-2 gene transcription. *J. Biol. Chem.* **277**, 33361-33368.

Gluhak-Heinrich, J., Yang, W., Harris, M. A. and Harris, S. E. (2008). Quantitative in situ hybridization with enhanced sensitivity in soft, bone and teeth tissue using Digoxigenin tagged RNA probes. *Biochem. Med.* **18**, 59-80.

Gluhak-Heinrich, J., Guo, D., Yang, W., Harris, M. A., Lichtler, A., Kream, B., Zhang, J., Feng, J. Q., Smith, L. C., Dechow, P. et al. (2010). New roles and mechanism of action of BMP4 in postnatal tooth cytodifferentiation. *Bone* **46**, 1533-1545.

Grcevic, D., Pejda, S., Matthews, B. G., Repic, D., Wang, L., Li, H., Kronenberg, M. S., Jiang, X., Maye, P., Adams, D. J. et al. (2012). In vivo fate mapping identifies mesenchymal progenitor cells. *Stem Cells* **30**, 187-196.

Jacobsen, K. A., Al-Aql, Z. S., Wan, C., Fitch, J. L., Stapleton, S. N., Mason, Z. D., Cole, R. M., Gilbert, S. R., Clemens, T. L., Morgan, E. F. et al. (2008). Bone formation during distraction osteogenesis is dependent on both VEGFR1 and VEGFR2 signaling. *J. Bone Miner. Res.* **23**, 596-609.

Kalajzic, Z., Li, H., Wang, L.-P., Jiang, X., Lamothe, K., Adams, D. J., Aguila, H. L., Rowe, D. W. and Kalajzic, I. (2008). Use of an alpha-smooth muscle actin GFP reporter to identify an osteoprogenitor population. *Bone* **43**, 501-510.

Kwon, T.-G., Zhao, X., Yang, Q., Li, Y., Ge, C., Zhao, G. and Franceschi, R. T. (2011). Physical and functional interactions between Runx2 and HIF-1α induce vascular endothelial growth factor gene expression. *J. Cell. Biochem.* **112**, 3582-3593.

Liu, F., Woitge, H. W., Braut, A., Kronenberg, M. S., Lichtler, A. C., Mina, M. and Kream, B. E. (2004). Expression and activity of osteoblast-targeted Cre recombinase transgenes in murine skeletal tissues. *Int. J. Dev. Biol.* **48**, 645-653.

Liu, Y., Berendsen, A. D., Jia, S., Lotinun, S., Baron, R., Ferrara, N. and Olsen, B. R. (2012). Intracellular VEGF regulates the balance between osteoblast and adipocyte differentiation. *J. Clin. Invest.* **122**, 3101-3113.

Lounev, V. Y., Ramachandran, R., Wosczyna, M. N., Yamamoto, M., Maidment, A. D., Shore, E. M., Glaser, D. L., Goldhamer, D. J. and Kaplan, F. S. (2009). Identification of progenitor cells that contribute to heterotopic skeletogenesis. *J. Bone Joint Surg. Am.* **91**, 652-663.

Maes, C., Goossens, S., Bartunkova, S., Drogat, B., Coenegrachts, L., Stockmans, I., Moermans, K., Nyabi, O., Haigh, K., Naessens, M. et al. (2010a). Increased skeletal VEGF enhances beta-catenin activity and results in excessively ossified bones. *EMBO J.* **29**, 424-441.

Maes, C., Kobayashi, T., Selig, M. K., Torrekens, S., Roth, S. I., Mackem, S., Carmeliet, G. and Kronenberg, H. M. (2010b). Osteoblast precursors, but not mature osteoblasts, move into developing and fractured bones along with invading blood vessels. *Dev. Cell* **19**, 329-344.

Maes, C., Carmeliet, G. and Schipani, E. (2012). Hypoxia-driven pathways in bone development, regeneration and disease. *Nat. Rev. Rheumatol* **8**, 358-366.

Martinez, M. D., Schmid, G. J., McKenzie, J. A., Ornitz, D. M. and Silva, M. J. (2010). Healing of non-displaced fractures produced by fatigue loading of the mouse ulna. *Bone* **46**, 1604-1612.

Matsubara, H., Hogan, D. E., Morgan, E. F., Mortlock, D. P., Einhorn, T. A. and Gerstenfeld, L. C. (2012). Vascular tissues are a primary source of BMP2 expression during bone formation induced by distraction osteogenesis. *Bone* **51**, 168-180.

McLeod, M. J. (1980). Differential staining of cartilage and bone in whole mouse fetuses by alcian blue and alizarin red S. *Teratology* **22**, 299-301.

Medici, D. and Olsen, B. R. (2012). The role of endothelial-mesenchymal transition in heterotopic ossification. *J. Bone Miner. Res.* **27**, 1619-1622.

Medici, D., Shore, E. M., Lounev, V. Y., Kaplan, F. S., Kalluri, R. and Olsen, B. R. (2010). Conversion of vascular endothelial cells into multipotent stem-like cells. *Nat. Med.* **16**, 1400-1406.

Moon, A. M., Boulet, A. M. and Capecchi, M. R. (2000). Normal limb development in conditional mutants of Fgf4. *Development* **127**, 989-996.

Nickel, W. (2003). The mystery of nonclassical protein secretion. A current view on cargo proteins and potential export routes. *Eur. J. Biochem.* **270**, 2109-2119.

Nyman, J. S., Lynch, C. C., Perrien, D. S., Thiolloy, S., O'Quinn, E. C., Patil, C. A., Bi, X., Pharr, G. M., Mahadevan-Jansen, A. and Mundy, G. R. (2011). Differential effects between the loss of MMP-2 and MMP-9 on structural and tissue-level properties of bone. *J. Bone Miner. Res.* **26**, 1252-1260.

Park, D., Spencer, J. A., Koh, B. I., Kobayashi, T., Fujisaki, J., Clemens, T. L., Lin, C. P., Kronenberg, H. M. and Scadden, D. T. (2012). Endogenous bone marrow MSCs are dynamic, fate-restricted participants in bone maintenance and regeneration. *Cell Stem Cell* **10**, 259-272.

Sacchetti, B., Funari, A., Michienzi, S., Di Cesare, S., Piersanti, S., Saggio, I., Tagliafico, E., Ferrari, S., Robey, P. G., Riminucci, M. et al. (2007). Self-renewing osteoprogenitors in bone marrow sinusoids can organize a hematopoietic microenvironment. *Cell* **131**, 324-336.

Schipani, E. and Kronenberg, H. M. (2008). Adult mesenchymal stem cells. In *StemBook*. Cambridge, MA: Harvard Stem Cell Institute.

Schipani, E., Maes, C., Carmeliet, G. and Semenza, G. L. (2009). Regulation of osteogenesis-angiogenesis coupling by HIFs and VEGF. *J. Bone Miner. Res.* **24**, 1347-1353.

Shu, B., Zhang, M., Xie, R., Wang, M., Jin, H., Hou, W., Tang, D., Harris, S. E., Mishina, Y., O'Keefe, R. J. et al. (2011). BMP2, but not BMP4, is crucial for chondrocyte proliferation and maturation during endochondral bone development. *J. Cell Sci.* **124**, 3428-3440.

Sieber, C., Kopf, J., Hiepen, C. and Knaus, P. (2009). Recent advances in BMP receptor signaling. *Cytokine Growth Factor Rev.* **20**, 343-355.

Singh, A. P., Castranio, T., Scott, G., Guo, D., Harris, M. A., Ray, M., Harris, S. E. and Mishina, Y. (2008). Influences of reduced expression of maternal bone morphogenetic protein 2 on mouse embryonic development. *Sex Dev.* **2**, 134-141.

Styrkarsdottir, U., Cazier, J. B., Kong, A., Rolfsson, O., Larsen, H., Bjarnadottir, E., Johannsdottir, V. D., Sigurdardottir, M. S., Bagger, Y., Christiansen, C. et al. (2003). Linkage of osteoporosis to chromosome 20p12 and association to BMP2. *PLoS Biol.* **1**, e69.

Tang, W., Yang, F., Li, Y., de Crombrugghe, B., Jiao, H., Xiao, G. and Zhang, C. (2012). Transcriptional regulation of Vascular Endothelial Growth Factor (VEGF) by osteoblast-specific transcription factor Osterix (Osx) in osteoblasts. *J. Biol. Chem.* **287**, 1671-1678.

Tsuji, K., Bandyopadhyay, A., Harfe, B. D., Cox, K., Kakar, S., Gerstenfeld, L., Einhorn, T., Tabin, C. J. and Rosen, V. (2006). BMP2 activity, although dispensable for bone formation, is required for the initiation of fracture healing. *Nat. Genet.* **38**, 1424-1429.

Tsuji, K., Cox, K., Bandyopadhyay, A., Harfe, B. D., Tabin, C. J. and Rosen, V. (2008). BMP4 is dispensable for skeletogenesis and fracture-healing in the limb. *J. Bone Joint Surg. Am.* **90 Suppl. 1**, 14-18.

Wang, Q., Huang, C., Xue, M. and Zhang, X. (2011). Expression of endogenous BMP-2 in periosteal progenitor cells is essential for bone healing. *Bone* **48**, 524-532.

Watabe, T. and Miyazono, K. (2009). Roles of TGF-beta family signaling in stem cell renewal and differentiation. *Cell Res.* **19**, 103-115.

Weinstein, R. S. (2010). Glucocorticoids, osteocytes, and skeletal fragility: the role of bone vascularity. *Bone* **46**, 564-570.

Weinstein, R. S., Wan, C., Liu, Q., Wang, Y., Almeida, M., O'Brien, C. A., Thostenson, J., Roberson, P. K., Boskey, A. L., Clemens, T. L. et al. (2010). Endogenous glucocorticoids decrease skeletal angiogenesis, vascularity, hydration, and strength in aged mice. *Aging Cell* **9**, 147-161.

Wohl, G. R., Towler, D. A. and Silva, M. J. (2009). Stress fracture healing: fatigue loading of the rat ulna induces upregulation in expression of osteogenic and

angiogenic genes that mimic the intramembranous portion of fracture repair. *Bone* **44**, 320-330.

Yang, W., Harris, M. A., Cui, Y., Mishina, Y., Harris, S. E. and Gluhak-Heinrich, J. (2012). Bmp2 is required for odontoblast differentiation and pulp vasculogenesis. *J. Dent. Res.* **91**, 58-64.

Yoon, B. S., Ovchinnikov, D. A., Yoshii, I., Mishina, Y., Behringer, R. R. and Lyons, K. M. (2005). Bmpr1a and Bmpr1b have overlapping functions and are essential for chondrogenesis in vivo. *Proc. Natl. Acad. Sci. USA* **102**, 5062-5067.

Zhang, H. and Bradley, A. (1996). Mice deficient for BMP2 are nonviable and have defects in amnion/chorion and cardiac development. *Development* **122**, 2977-2986.

Zhang, F., Qiu, T., Wu, X., Wan, C., Shi, W., Wang, Y., Chen, J. G., Wan, M., Clemens, T. L. and Cao, X. (2009). Sustained BMP signaling in osteoblasts stimulates bone formation by promoting angiogenesis and osteoblast differentiation. *J. Bone Miner. Res.* **24**, 1224-1233.

Zhang, R., Oyajobi, B. O., Harris, S. E., Chen, D., Tsao, C., Deng, H.-W. and Zhao, M. (2013). Wnt/β-catenin signaling activates bone morphogenetic protein 2 expression in osteoblasts. *Bone* **52**, 145-156.

Zhao, M., Harris, S. E., Horn, D., Geng, Z., Nishimura, R., Mundy, G. R. and Chen, D. (2002). Bone morphogenetic protein receptor signaling is necessary for normal murine postnatal bone formation. *J. Cell Biol.* **157**, 1049-1060.